Articles

Alternative Binding Modes of Proline-Rich Peptides Binding to the GYF Domain†

Wei Gu,‡ Michael Kofler,§ Iris Antes,|| Christian Freund,*,§ and Volkhard Helms*,‡

Zentrum für Bioinformatik, Universität des Saarlandes, D-66041 Saarbrücken, Germany, Protein Engineering Group, Forschungsinstitut für Molekulare Pharmakologie and Freie Universität Berlin, D-13125 Berlin, Germany, and Max-Planck-Institut für Informatik D-66123 Saarbrücken, Germany

Received September 17, 2004; Revised Manuscript Received March 14, 2005

ABSTRACT: Recognition of proline-rich sequences plays an important role for the assembly of multiprotein complexes during the course of eukaryotic signal transduction and is mediated by a set of protein folds that share characteristic features. The GYF (glycine-tyrosine-phenylalanine) domain is known as a member of the superfamily of recognition domains for proline-rich sequences. Recent studies on the complexation of the CD2BP2-GYF domain with CD2 peptides showed that the peptide adopts an extended conformation and forms a polyproline type-II helix involving residues Pro4−Pro7 [Freund et al. (2002) *EMBO J. 21*, 5985−5995]. R/K/GxxPPGxR/K is the key signature for the peptides that bind to the GYF domain [Kofler et al. (2004) *J. Biol. Chem. 279*, 28292−28297]. In our combined theoretical and experimental study, we show that the peptides adopt a polyproline II helical conformation in the unbound form as well as in the complex. From molecular dynamics simulations, we identify a novel binding mode for the G8W mutant and the wild-type peptide (shifted by one proline in register). In contrast, the conformation of the peptide mutant H9M remains close to the experimentally derived wild-type GYF−peptide complex. Possible functional implications of this altered conformation of the bound ligand are discussed in the light of our experimental and theoretical results.

Intracellular protein domains recognizing proline-rich sequences (PRS)[1] play a pivotal role in biological processes that require the coordinated assembly of multiprotein complexes (*1*). In vertebrate genomes, PRS are predicted to be among the most abundantly expressed amino acid sequence motifs (*2*), and this corresponds to an increasing number of proteins that acquired PRS-recognition domains during the course of evolution (*3*).

Up to now, the superfamily of PRS-recognition domains consists of profilin (*4*), SH3 (*5*, *6*), WW (*7*), EVH1 (*8*), GYF (*9*, *10*), UEV (*11*, *12*), and probably the ligand-binding domain of prolyl-4-hydroxylase (*13*). For each of these domains, a set of conserved aromatic amino acid residues is important for peptide binding. Within the glycine-tyrosine-phenylalanine (GYF) domain, the GYF tripeptide is part of a bulge−helix−bulge motif that contains several aromatic amino acid side chains that are essential for the binding of the CD2 cytoplasmic domain. The recently solved NMR structure of the CD2BP2-GYF domain in complex with the CD2 peptide SHRPPPPGHRV (*14*) showed that the peptide adopts an extended conformation and forms a left-handed polyproline type-II (PPII) helix involving residues Pro4−Pro7 (*14*, *15*) (see Figure 1). The binding surface of the GYF domain accommodates Pro6 and Pro7 of the ligand and is defined primarily by the aromatic residues Tyr6, Trp8, Tyr17,

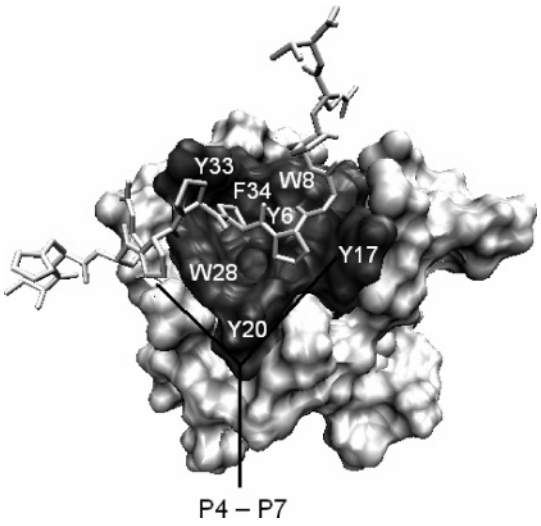

FIGURE 1: NMR structure of GYF domain with wild-type peptide. The GYF domain is represented by its molecular surface; the peptide atoms are drawn as sticks. Residues forming the binding pocket are colored in dark gray and labeled by their one-letter codes and sequence numbers. The VMD (*60*) package was used to generate this picture.

† This work was supported by Grants I177955 and I177956 from the Volkswagen Foundation.

* To whom correspondence should be addressed. Telephone: 49 681 302 64165. Fax: 49 681 302 64180. E-mail: volkhard.helms@bioinformatik.uni-saarland.de (V.H.); Telephone: 49 30 94793 181. Fax: 49 30 94793 189. E-mail: freund@fmp-berlin.de (C.F.).

‡ Universität des Saarlandes.

§ Forschungsinstitut für Molekulare Pharmakologie and Freie Universität Berlin.

|| Max-Planck-Institut für Informatik.

[1] Abbreviations: GYF, glycine-tyrosine-phenylalanine; PRS, proline-rich sequence; NOE, nuclear Overhauser effect.

10.1021/bi0479914 CCC: $30.25 © 2005 American Chemical Society
Published on Web 04/07/2005

Scheme 1

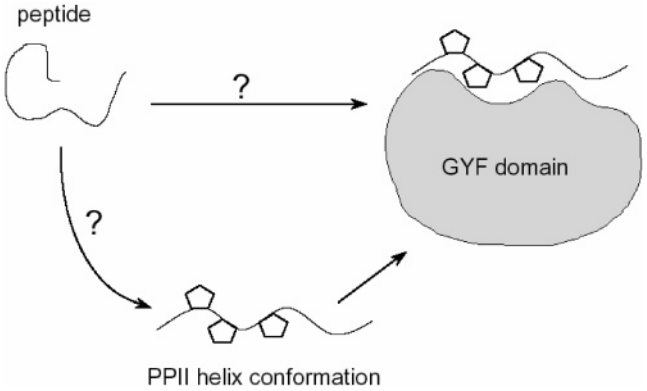

Tyr20, Trp28, Tyr33, and Phe34 of the GYF domain (see Figure 1).

Characterizing the conformational changes for both interaction partners is essential for understanding the mechanism of the peptide binding to the GYF domain. On one hand, it has been recently recognized that many proteins contain long disordered segments in their functional states under usual physiological conditions (*16*−*20*); e.g., most of the polypeptide hormones are conformationally disordered in aqueous solution and fold upon binding to their receptors (*20*). Unstructured segments within large proteins provide ideal scaffolds for the interaction with several different targets and thereby help to assemble multiprotein complexes (*16*−*20*). On the other hand, it has been shown by many experimental and theoretical studies that certain peptides, including proline-rich sequences, adopt preferred conformations in solution (*1*, *21*−*31*). Therefore, it is a matter of ongoing discussion whether the PPII helix is such a preferred conformation of certain peptide sequences (*21*, *25*, *27*−*29*, *32*−*39*). In the CD2 polyproline peptide−GYF complex, the central part of the peptide adopts a PPII helical conformation. A mechanistic description of the binding event has to distinguish whether the PPII helix conformation is preformed in the unbound peptides and binding to the GYF domain takes place in a "lock and key" mode or whether folding and binding occurs in parallel, corresponding to an "induced fit" model (Scheme 1). Further, it should clarify which conformational changes take place in the protein and peptide and how these changes contribute to the stabilization of the complex. So far, our previous study has identified the key binding motif of the peptide as R/K/GXXPPGXR/K (*40*). The structural importance of peptide Gly8 for interaction with the GYF domain has also been analyzed (*14*): A glycine in this position terminates the PPII helix conformation and prevents hindrance between the C terminus of the peptide and the domain. A G8X mutation resulted in the loss of binding for most residues during systematic mutagenetic studies (see Table 1). Surprisingly, the peptide still binds to the domain upon a G8W mutation (*40*), although, on the basis of the wild-type structure, a G8W substitution would result in a clash between the tryptophane and the GYF domain. Considering the large structural differences between glycine and tryptophan, a different binding mode for this peptide can be assumed. It has been shown by NMR experiments (*41*) that SH3 domains can bind proline-rich ligands in two orientations, because of the pseudosymmetry of the PPII helix. These findings raised the question whether such a scenario is also true for the GYF domain.

Table 1: Favorable Mutations of the Peptides Binding to GYF Domain[a]

WT	A	C	D	E	F	G	H	I	K	L	M	N	P	Q	R	S	T	V	W	Y
S	+	+			+	+	+	+	+	+	+	+	+	+	+	+	+	+	+	+
H	+	+			+	+	+	+	+	+	+	+	+	+	+	+	+	+	+	+
R						+			+						+					
P	+	+			+	+	+	+	+	+	+	+	+	+	+	+	+	+	+	+
P	+					+							+							
P													+							
P						+							+							
G						+									+				+	
H	+	+			+	+	+	+	+	+	+	+	+	+	+	+	+	+	+	+
R									+						+					
V	+				+	+	+	+	+	+	+	+	+	+	+	+	+	+		+

[a] Data are taken from Kofler et al. (*40*). Mutations favorable for the binding are marked "+". The first column labeled "WT" contains the sequence of the wild-type peptide. The later columns contain the results from single amino acid mutation experiments. Amino acid residues are listed with their one letter code.

In the present work, we carried out theoretical calculations to address the problem of the conformational state of unbound peptides. Molecular dynamics (MD) simulations starting from different initial conformations and at different temperatures indicated that all studied peptides adopt the PPII helical conformation in the unbound state. For the wild-type and G8W mutant peptides, we combined NMR experiments with theoretical calculations and identified a novel binding mode (register shifted by one proline), while the control peptide mutant H9M remains close to the experimental GYF-domain wild-type peptide complex conformation (*14*). Possible functional implications of this altered conformation of the bound ligand are discussed in the light of our experimental and theoretical results.

MATERIALS AND METHODS

Protein Production and NMR Analysis. The GYF domain of human CD2BP2 comprising amino acids 280−342 was cloned and expressed as described elsewhere (*40*). The NMR experiments were performed at 296 K using a Bruker DRX600 instrument equipped with a standard triple-resonance probe. Data processing and analysis were carried out using the XWINNMR (Bruker) software package and the program Sparky (*42*). In the NMR experiments, increasing amounts of the synthetic peptide of sequence NH_2-SHRPPPPGHRV-COOH or NH_2-SHRPPPPWHRV-COOH were added to a 0.2 mM sample of the ^{15}N-labeled GYF domain up to a final concentration of 1.8 mM. HSQC spectra were recorded, and the changes of the assigned nitrogen and hydrogen chemical shifts were combined as follows: $[(\Delta^1H\_cs)^2 + (\Delta^{15}N\_cs)^2]^{1/2}$, where Δ^1H_cs is the chemical-shift change for ^{1}H atoms in units of 0.1 ppm and $\Delta^{15}N\_cs$ is the chemical-shift change for ^{15}N atoms in units of 0.5 ppm. The sum of these weighted geometrical differences of the chemical shifts were plotted against the peptide concentrations for the titration experiments. The resonances of residue F34 and of the W8 side chain were excluded because of line broadening preventing the identification of the corresponding resonances at various ligand concentrations. The dissociation constants were calculated using the program Microcal Origin. For comparison of the two binding epitopes, the weighted geometrical differences of the chemical shifts for all assigned residues upon addition of 1.8 mM ligand are shown in a histogram.

Table 2: Summary of All of the Simulations

simulation	system	starting structure	*T* (K)	length (ns)
WT	wild-type peptide	NMR structure	300	20
WTE	wild-type peptide	modeled extended structure	300	20
WTHT	wild-type peptide	NMR structure	500	20
G8W	G8W mutant peptide	modeled from NMR	500	40
H9M	H9M mutant peptide	modeled from NMR	500	40
WT_GYF	wild type + GYF	NMR structure	300	30
G8W_GYF	G8W mutant + GYF	modeled from NMR and simulation	300	30
H9M_GYF	H9M mutant + GYF	modeled from NMR and simulation	300	30
G8W_DOCK	G8W mutant + GYF	docking based on NMR	300	30
G8R_DOCK	G8R mutant + GYF	docking based on NMR	300	30
G8Y_DOCK	G8Y mutant + GYF	docking based on NMR	300	30
G8K_DOCK	G8K mutant + GYF	docking based on NMR	300	30
ALT_GYF	wild type + GYF	modeled from NMR and simulation	300	5*20

Peptide Substitution Analysis. Single substitutions of SHRPPPPWHRV and a set of different proline-rich peptides were generated by semiautomated spot synthesis (*43*, *44*) (Abimed; Software LISA, Jerini AG) on Whatman 50 cellulose membranes as described (*45*). Membranes were probed with GST fusion protein as described elsewhere (*46*). Briefly, the membranes were incubated with GST−GYF (CD2BP2; 40 μg/mL) overnight. After washing, bound GST fusion protein was detected with rabbit polyclonal anti-GST antibody (Z-5, Santa Cruz) and horseradish peroxidase coupled anti-rabbit IgG antibodies (Rockland). An enhanced chemiluminescence substrate (SuperSignal West Pico, Pierce, IL) on a LumiImagerTM (Boehringer Mannheim GmbH) was used for detection.

Molecular Dynamics Simulations: Peptides. To characterize the conformational ensembles of the unbound solvated peptides, a set of MD simulations of the wild-type (SHRPPPPGHRV) and the mutated peptides (SHRPPPPWHRV and SHRPPPPGMRV) were carried out using the GROMACS3.14 package (*47*) applying the OPLSAA force field (*48*). In some cases, the starting structures were taken from the complex of the wild-type peptide with the GYF domain [PDB entry 1L2Z (*14*)]. Three MD simulations of the wild-type peptide were performed: (1) start from the wild-type NMR structure at 300 K temperature (WT); (2) start from a modeled extended structure at 300 K temperature (WTE); (3) start from the NMR structure at a temperature of 500 K (WTHT). The extended conformation in the WTE simulation was generated with dihedral angles of the backbone of 135° (N−CA−C−N), 180° (CA−C−N−CA), and −135° (C−N−CA−C). MD simulations of the mutated peptides (G8W for SHRPPPPWHRV and H9M for SHRPPPPGMRV) were performed only at 500 K. Mutated residues (tryptophan in the G8W simulation and methionine in the H9M simulation) were modeled using the TINKER package (*49*) based on the NMR structure of the wild-type peptide in the complex. The peptides were solvated in cubic boxes, using TIP3P water molecules (*50*), with an initial minimum distance of at least 14 Å between the boundaries of the box and the nearest solute atom. All coordinate sets were first minimized by 500 steps of steepest-descent energy minimization. The solvent and protein atoms were then relaxed during a 100 ps MD simulation with all non-hydrogen atoms of the NMR structure restrained to their coordinates in the PDB structure. Then, plain MD simulations (20 ns for WT, WTE, and WTHT and 40 ns for G8W and H9M) were carried out without any restraints. The LINCS procedure (*51*) was applied to constrain all bond lengths. The time step of the simulation was set to 2 fs. A 9 Å cutoff was used for the short-range nonbonded interactions, and the lists of nonbonded pairs were updated every 10 steps. The particle mesh Ewald (PME) method (*52*) with a grid size of 1.2 Å was used to calculate long-range electrostatic interactions. Temperature and pressure were maintained by weak coupling to an external bath in the simulations (*53*). Cluster analysis was carried out after the simulations using the "full linkage" algorithm implemented in the GROMACS3.14 package (*47*): a structure is added to an existing cluster when its distance to any element of the cluster is less than the given cutoff. Main-chain atoms and C_β atoms were selected for calculating the root-mean-square deviation (rmsd) matrix. The rmsd cutoff was set to 1.5 Å.

Complexes. The dominant conformations in the cluster analysis of each simulation of the unbound mutated peptides G8W and H9M were superimposed on the wild-type peptide in the structure of the complex using all main-chain atoms (backbone, H, and O) and the C_β atoms of the HRPPPP segment for alignment. Then, 500 steps of steepest-descent energy minimization were applied to remove unfavorable interactions. The two optimized mutated complexes were used as starting structures in the simulations of the mutant complexes. Similar procedures as for the peptide simulations were used to carry out two 30 ns long MD simulations of the modeled complexes at 300 K (G8W_GYF for the peptide SHRPPPPWHRV and the GYF domain and H9M_GYF for the peptide SHRPPPPGMRV and the GYF domain). To investigate the binding mode of the G8X mutations more systematically, we used the package FlexX (*54*) to dock the G8W, G8R, G8Y, and G8K mutants to the GYF domain followed by subsequent MD simulations. Pro7 of the peptide was chosen as a seed in the docking, while the complex conformations with the best docking score were chosen as the starting structures of the simulations. MD simulation of the wild-type complex was also carried out as a control run (WT_GYF). Details about all simulations (starting structure, temperature, and length) reported here are summarized in Table 2.

RESULTS

Solvent Conformation of the Unbound Peptide. As described in the Materials and Methods, the molecular dynamics simulations for the wild-type peptide were started from different starting conformations of the peptide (a PPII helical conformation taken from the NMR complex and a modeled extended starting conformation) at two different temperatures

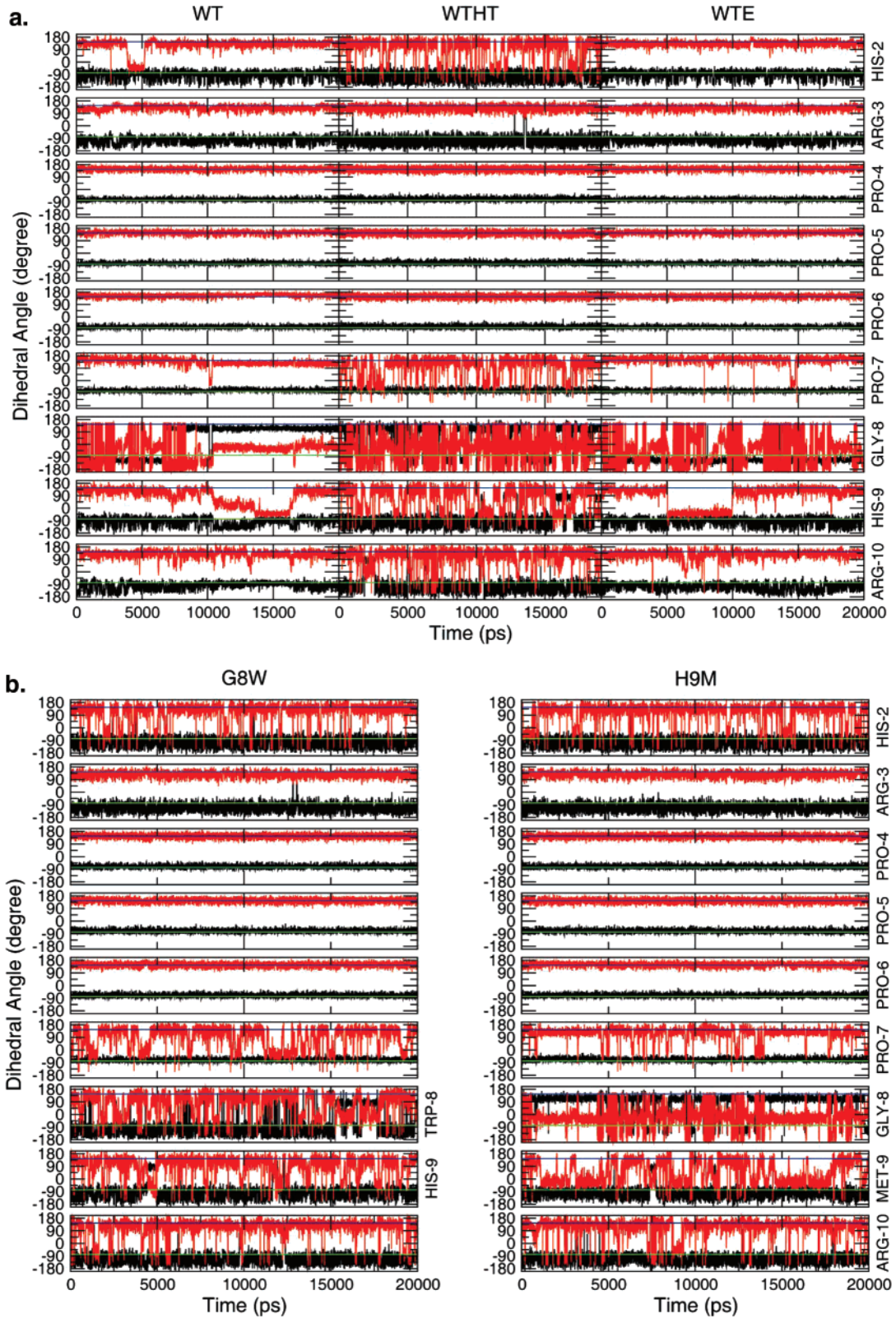

FIGURE 2: Evolution of the backbone dihedral angles (black, ϕ angles; red, ψ angles) during the simulation of the wild-type peptide (a) and the mutant peptide (b). Ideal values of the dihedral angles are shown in solid lines (blue, ϕ angles; green, ψ angles).

(300 and 500 K). Figure 2 shows the evolution of backbone dihedral angles (Φ, Ψ) during the 20 ns long simulations. In the WTE run, the formation of the PPII helical conformation occurred after only a few picoseconds. Therefore, this initial conformation cannot be resolved in Figure 2a. In all three simulations of the wild-type peptide (shown in Figure 2a), the backbone dihedral angles of residues His2−Pro7 merely fluctuated around the ideal value for PPII helix: $\Phi = -78°$, $\Psi = 146°$ (*55*). The simulation at high temperature (WTHT) shows only slight shifts, where the segment Gly8−Val11 contributes to most of the fluctuation of the backbone conformation. Similar results were also found in the simulations of the mutated peptides G8W and H9M (shown in Figure 2b).

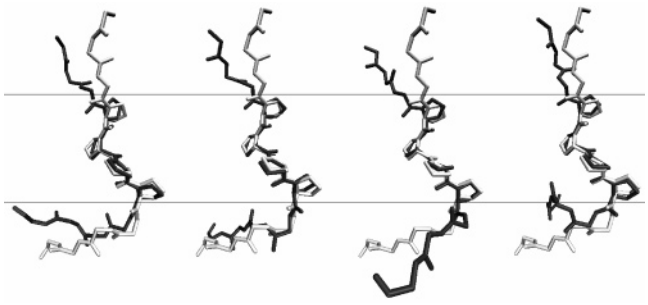

FIGURE 3: Superposition of the representative conformations of simulations of unbound peptides (from left to right: WT, WTE, G8W, and H9M) onto the bound peptide in the NMR structure. Representative conformations are colored in black, while the bound peptide in the NMR structure is shown in gray.

After this initial comparison between the simulations of wild-type and mutated peptide, the G8W and H9M simulations were extended to 40 ns to improve the sampling of the conformational space of the mutated peptides and to allow for identification of possible interesting peptide conformations that could be used for the modeling of the mutated complexes. We used cluster analysis to summarize the sampling during the simulation of G8W and H9M. Interestingly, only one dominant cluster was found in each simulation: the largest cluster covers 77 and 86% of the trajectory in the G8W and H9M simulation, respectively. A similar observation was made for the simulations of the wild-type peptide: only one cluster was found in the analysis, which covers almost the whole trajectory. These results agree with the dihedral angle analysis that the backbones of the mutated and wild-type peptides are quite stable during the simulation.

Figure 3 shows a superposition of representative conformations of each simulation (WT, WTE, G8W, and H9M) onto the bound peptide of the NMR structure. It is clearly visible that the PPII helix conformation is adopted in all cases. The conformations of Pro4−Pro7 overlap very well with each other, and deviations only appear at the two termini of the peptides. The stable PPII helix conformation found in all simulations indicates that all three peptides are able to adopt a PPII helix conformation in the unbound state and is reflected by the occurrence of one dominant cluster. This is in agreement with previous theoretical and experimental studies on polyproline peptides (*1*, *21*, *23*−*26*). Rucker and Creamer explained the bias of polypeptide folding into the PPII helix as an energetically favorable option: all backbone polar groups are well-solvated in this conformation in water, thus compensating for the lack of intramolecular hydrogen bonds (*28*).

Binding Analysis of the GYF Domain to the Mutated and Wild-Type Peptides. Binding analysis and combined chemical-shift changes were measured by NMR experiments for the G8W peptide as well as for the wild-type peptide binding to the CD2BP2-GYF domain. The results are shown in parts a−c of Figure 4. The spectra and therefore the chemical-shift changes of the GYF domain in complex with wild-type peptide (SHRPPPPGHRV) and the mutated peptide G8W (SHRPPPPWHRV) are very similar. Because the chemical shift is a very sensitive measure of the chemical environment, the precise overlap for almost all resonances except Trp8 in both spectra (Figure 4b) surprisingly demonstrates that the binding surface of the GYF domain is very similar for the two peptides. The pattern of chemical-shift changes (Figure 4c) reveals the binding face for the polyproline peptide on the GYF domain. Most of the strongly shifted resonances belong to residues that are highly conserved among putative GYF domains (*14*) and are almost identical for the two peptides. However, a large chemical-shift change was found for the backbone NH of W8 (Figure 4b). This result illustrates that conformational changes because of the G8W mutation happen near this residue, while for other residues, the chemical-shift changes are quite similar between the GYF domains binding to the wild-type peptide and the G8W mutant. Actually, the G8W peptide binds with a slightly lower affinity. Assuming a two-state binding model for the peptides, apparent K_D values of 220 ± 30 and 290 ± 20 μM were determined by NMR for the wild-type and the mutant peptide, respectively.

Structure of the Complex with the Mutated Peptide. To investigate the conformational changes of the complex, which are due to single mutations of peptide residues, we first modeled both mutant complexes: Gly8 to Trp (G8W_GYF) and His9 to Met (H9M_GYF). In the G8W_GYF complex, the mutated residue Gly8 is very important for the binding of the peptide, while in the second case, the mutated residue His9 is not crucial for the binding affinity as shown by systematic mutational analysis (Table 1). Considering that the mutated peptides only adopt one dominant conformation for their polyproline regions and that the mutations were introduced only near the C terminus, we superimposed the mutated peptides on the wild-type peptide using the PPII helix and the N-terminus segment, thereby modeling the initial structure of the mutated complexes based on the superposition.

Overview of the Simulations. The two modeled mutant complexes were first optimized by 500 steps of steepest-descent energy minimization. However, energy minimization is not enough to provide a complete picture of the properties and stabilities of the predicted structures and should be complemented by unconstrained MD simulations. The rmsd values with respect to the starting and final coordinate sets of the C_α atoms are very stable and center around 2 Å in the simulations of the wild-type (WT_GYF) and the H9M mutant (H9M_GYF) complex. For the G8W_GYF complex, however, the rmsd values of the simulation are significantly smaller with respect to the final coordinates compared to the initial coordinates (2 and 3−3.5 Å, respectively). This indicates that the modeled starting conformation is not stable and some conformational changes occurred during the simulation, while the final structure is more stable and closer to the "central" conformations of the simulations.

A more systematical way of characterizing the conformations is the before mentioned cluster analysis. Main-chain and C_β atoms were selected for calculating the rmsd matrix. The rmsd cutoff was set to 1.0 Å. This cutoff is smaller than that used for the MD simulations of the peptides (1.5 Å). Nevertheless, a few dominant clusters cover most of the trajectory: in the G8W_GYF simulation, the two largest clusters cover 81% of the trajectory (46 and 35%, respectively) and the remaining 18 clusters share the remaining 19%, while in the H9M_GYF simulation, only one large cluster was found, which covers almost 99% of the trajectory. In the superimposed model of the G8W_GYF complex, a new pocket is opened by Trp8, Glu9, Tyr17, and Phe20 of the domain. It seems that this pocket accommodates the large

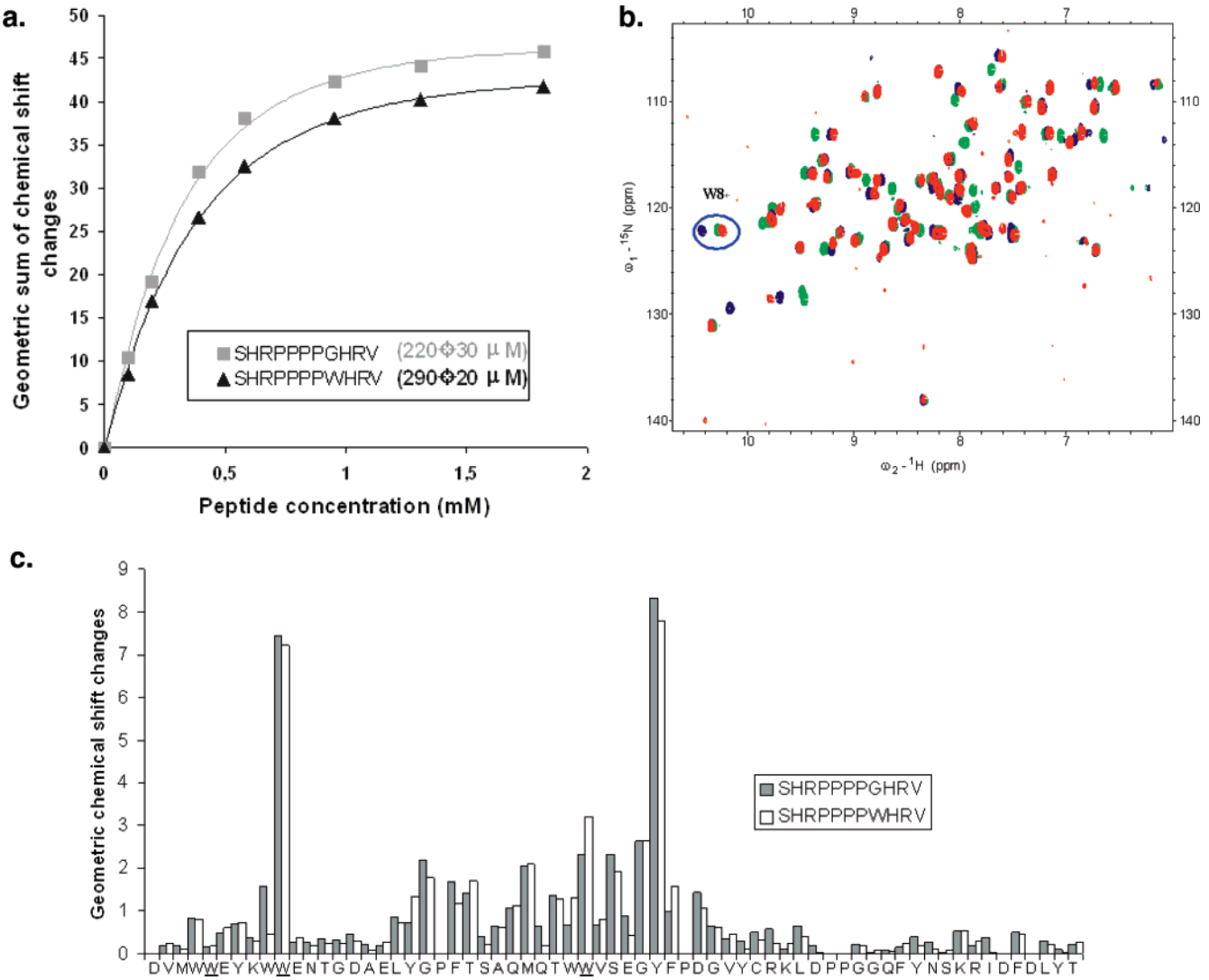

FIGURE 4: Binding analysis of the CD2BP2-GYF domain to the peptide SHRPPPPWHRV in comparison to the wild-type peptide SHRPPPPGHRV by NMR. (a) Sum of the weighted geometrical differences of the chemical shifts (geometric sum of chemical-shift changes) for assigned peaks, which could be identified at all applied peptide concentrations, is plotted against the concentration of the peptide. (b) Mapping of the binding site of SHRPPPPGHRV and SHRPPPPWHRV peptides onto the CD2BP2-GYF domain. Overlay of HSQC spectra of GYF domain alone (green) and GYF domain in the presence of a 10-fold excess of the wild-type peptide SHRPPPPGHRV (blue) or the mutant peptide SHRPPPPWHRV (red), respectively. A quantitative analysis of the chemical-shift changes of each residue is presented as a histogram (c). The weighted geometrical differences of the chemical shifts for each assigned residue upon addition of a 10-fold excess of peptide are plotted against the corresponding residue. Prolines are depicted for completeness. The weighted geometrical differences of the chemical shifts of tryptophan side chains are indicated by W.

side chain of Trp8 of the peptide and therefore avoids clashes. However, this binding mode was not stable in the simulation, and the side chain of peptide residue Trp8 finally moved out of this pocket after 12 ns, pointing toward the solvent where it finally reached an equilibrated state. This change is also reflected by the cluster analysis: two large clusters were found in the simulation, each representing one state of the Trp8 side chain. The cluster in which the side chain of peptide Trp8 stays in the pocket covers most of the trajectory between 0 and 12 ns (35% of the total and 87% of 0−12 ns), while the other one in which Trp8 moved out covers most of the remaining part (46% of the total and 77% of 12−30 ns).

Docking Experiments. To investigate the binding mode of the G8X mutations more systematically, we docked G8W, G8R, G8Y, and G8K mutants to the GYF domain using the FlexX program for flexible ligand docking and then carried out MD simulations (G8X_DOCK). The G8W and G8R mutations are the only mutations that were experimentally confirmed to be favorable in this position (Table 1). The G8Y and G8K mutants were chosen to mimic G8W and G8R as control cases. After docking, the side chains of the mutated residue (G8X) pointed to the solvent in all cases, implicating that the prolines are shifted by one position. This "shift in register" is in agreement with the experimental structure of the complex (used for the docking) that seems not to allow larger side chains at the position of Gly8. In the G8W_DOCK simulation, a contact was found between the side chain of Trp8 of the peptide and the side chain of Trp8 of the GYF domain. The distance between the center of mass of the two side chains was 5.9 ± 1.1 Å during the 30 ns MD simulation. The same contact was also found for the G8R_DOCK simulation, where the distance between the center of mass of Arg8 (peptide) and Trp8 (GYF domain) was 4.3 ± 0.5 Å during the simulation. For the G8K_DOCK simulation, this contact is formed only during the first 5 ns of the simulation

and is finally lost in the remaining simulation (5−30 ns). The distance between the center of mass of the corresponding residues shifted from 4.6 ± 0.8 Å (0−5 ns) to 11.2 ± 1.3 Å (5−30 ns). In the G8Y_DOCK simulation, no contact between Tyr8 of the peptide and any residues in the GYF domain was found during the entire simulations. The average distance between the center of mass of Tyr8 (peptide) and Trp8 (GYF domain) was 12.9 ± 1.5 Å.

DISCUSSION

Preformation of the PPII Helix. For many proteins with unstructured segments, the coupling of binding and folding is favorable according to the binding free energy: the entropic penalty associated with the folding transition is counterbalanced by a large enthalpy of binding (*16*, *56*). In those cases, the folding upon binding acts as a fine controller of the thermodynamics balance. In contrast, the polyproline peptides in our study are already folded into a PPII helix conformation in the unbound state and bind constitutively to the GYF domain. This binding mode is entropically more favorable than binding of unstructured peptides. The rigid PPII helix conformation of the unbound peptides studied is intrinsically stable in solution and is also favorable for its specific binding motif. Hilser and colleagues studied binding of the polyproline Sos peptide to the Sem-5 SH3 domain (*21*). They found that the PPII bias of unstructured peptides is driven by a favorable and significant enthalpy (ΔH) of -1.7 kcal mol^{-1} residue^{-1}, which is partially offset by an unfavorable entropy ($T\Delta S$) of -0.7 kcal mol^{-1} residue^{-1}, relative to the ensemble of disordered conformation of the molecule. A similar example is the c-Myb oncoprotein, which folds into an α-helical conformation both complexed and uncomplexed with its target protein (*56*). Remarkably, binding of c-Myb to its target (residue 586−672 of CREB-binding protein) is entropically favored ($\Delta S = +7.5$ cal mol^{-1} K^{-1}), while its favorable enthalpy change is small ($\Delta H = -4.1$ kcal mol^{-1} K^{-1}) (*16*, *56*).

It has been proposed by Dyson and Wright that unstructured proteins provide a large flexibility of binding reactions because they may adopt various structures upon binding to different partners (*20*). On the other hand, as examplified here for the GYF domain−ligand pair, the preformation of a peptide conformation might be well-suited to guarantee the rapid formation of specific peptide−protein complexes within the dynamic settings of signal transduction.

Analysis of the Binding Modes: H9M_GYF Agrees with the Wild Type. The results from the cluster analysis of the simulations as well as the NMR structures were used for comparing the binding modes for different mutations. Figure 5 shows the binding interfaces as well as the peptide of the wild-type complex (NMR and simulation) and that of the H9M mutant with the GYF domain. The hydrophobic pocket formed by Trp8, Tyr17, Phe20, Trp28, and Tyr33 of the GYF domain is structurally maintained to accommodate Pro6 and Pro7 of the peptide in the simulations of WT_GYF and H9M_GYF, in agreement with the NMR-derived structure. Arg3 and Arg10 of the peptide stay close to Glu31 and Glu9 of the domain. We conclude that favorable hydrophobic interactions between Pro6, Pro7, and the pocket, together with the electrostatic attraction between the positively charged residues Arg3 and Arg10 of the peptide and the negatively charged residues Glu31 and Glu9 of the domain

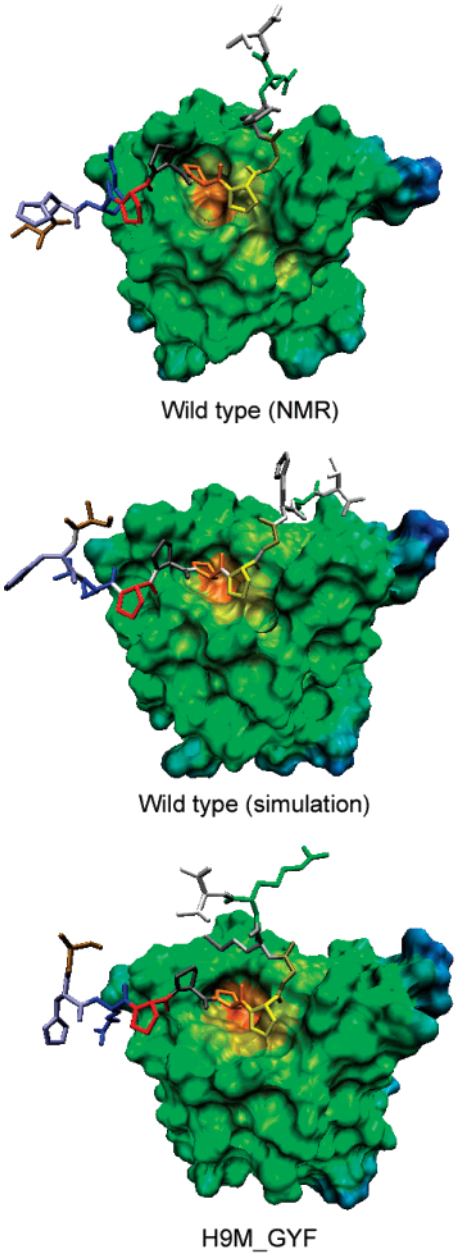

FIGURE 5: Comparison of the binding interfaces of the GYF domain (NMR and simulation) for the wild-type complex (above) and the H9M mutant (below). The GYF domain is represented by its molecular surface and colored by position (from orange to deep blue: completely buried to completely exposed); the peptide atoms are drawn as sticks and colored according to their appearance in the sequence.

play a central role for binding. These observations are consistent with the results from the substitution analysis; any mutation among these residues induces an unbinding of the peptide, and the only tolerated substitutions are to glycine or lysine and to lysine for Arg3 and Arg10, respectively (see Table 1). Other important interactions present in all simulations as well as in the NMR experiments are the hydrogen bonds between the backbone oxygens of peptide Pro4 and Pro7 and the side-chain H_ϵ in the domain. However, these hydrogen-bonding interactions do not bring any specificity for Pro4 in that position because most substitutions are tolerated (see Table 1). This can be explained by the fact that the H_α of Pro4 points into solution and no replacement should cause clashes with other residues or influence the

formation of this hydrogen bond. For Pro7, the specificity is the consequence of the hydrophobic interaction with the binding pocket of the GYF domain.

In the WT_GYF and H9M_GYF simulations, the binding interfaces do not show significant differences with respect to the NMR structure. The small rmsd in these two simulations also indicate that the wild-type peptide and the H9M mutant bind to the GYF domain in a similar fashion. The terminal residues (Ser1, His2, His9, and Val11) are not involved in hydrophobic or electrostatic interactions that are crucial for the binding in either the NMR structure or conformations sampled in the simulations. Therefore, we conclude that the tolerated mutations of these positions will not change the binding interface of the GYF domain significantly and the mutated peptides will bind to the domain analogously to the WT peptide.

G8X_DOCK: New Binding Modes. In the cluster analysis of the G8W_DOCK simulation, two large clusters were found: the first cluster covers the first 12 ns of the simulation, while the second covers the simulation from 12 to 30 ns. Figure 6a shows the superposition of the representative conformations of each cluster. The most important differences between the two clusters are that the interacting prolines in the peptide are shifted one position: Pro5 and Pro6 now insert into the binding pocket instead of Pro6 and Pro7. All four prolines in the peptide are rotated clockwise when viewed from the C to the N terminal. Interestingly, the orientations of the remaining residues were kept and show only a sight translation toward the C terminus. When looking at the interactions between the peptides and the GYF domain, the electrostatic attraction between the positively charged residues Arg3 and Arg10 of the peptide and the negatively charged residues Glu31 and Glu9 of the domain were maintained in both clusters. The hydrogen bonds between the backbone oxygen of peptide Pro4 and H_ϵ of the domain Trp28 side chain and between the backbone oxygen of peptide Pro7 and H_ϵ of the domain Trp8 side chain were kept in the first cluster, while the acceptor atoms were shifted to peptide Arg3 and peptide Pro6 in the second cluster as a consequence of the translation. To obtain experimental backup for this proposed binding mode, a peptide substitution analysis with the SHRPPPPWHR peptide was performed. In this experiment, each amino acid of the peptide is individually exchanged against all other naturally occurring amino acids. Thereby, the contribution of individual amino acids to the binding event can be estimated. Figure 7 shows the result of this experiment. Clearly, the importance of the PPW motif is suggested by the observed spot intensities, because mutations at these positions are mostly not compatible with detectable interactions. Furthermore, the second proline of the motif, which is exposed to the solvent when bound in the original wild-type conformation, also shows considerable conservation. This is in agreement with the alternative binding mode suggested by the MD simulations. The second proline in the new binding mode would now contact the domain directly and thereby contribute to binding.

To further validate this new finding, we also performed a cluster analysis on the G8R_DOCK simulation. The same motion was also found in this simulation, and the main conformation occupying the entire 30 ns was similar to the shifted register binding observed in the second cluster of the G8W_DOCK simulation (see Figure 6b), supporting our results.

Implications of the Alternative Binding Modes. To investigate the function of this alternative binding mode in depth and to test whether it only occurs for mutant peptides, we carried out five 20 ns MD simulations (ALT_GYF) of the wild-type complex starting from the same register shifted mode found in the second cluster of the G8W_DOCK simulation with different random seeds for the generation of initial atomic velocities. While the systems' overall behavior may be a bit different (the C_α rmsd with respect to the starting coordinates are stable around 2 Å in four simulations but reached 3−3.5 Å in the fifth simulation because of some structural changes at the C terminus of the GYF domain), interestingly, the alternative binding mode of the peptide is well-maintained in all five simulations of the wild-type complex. In cluster analyses carried out after the simulations, only one dominant cluster was found in each simulation. An overlap of all of the representative conformations is shown in Figure 6c. Although some lateral movements are observed between the individual conformations (in part because of different relative positions of the GYF domain used for superposition), note that Pro7 never shifts to the position of Pro6. Knowing that polyproline peptides bind to SH3 domains in both directions, we believe that the motion found in the G8W_DOCK and G8R_DOCK simulations is probably because of a transition between two alternative binding modes. This "screw-like" rotation−translation motion (Figure 6d) or the transition between different binding modes can decrease the entropic penalty of the binding without affecting the specificity. Providing two alternative binding modes for a peptide should, theoretically, provide additional stability for the bound conformation because of the larger number of states accessible inside the minimum energy well of the bound state (Figure 8). Another possible function of this motion may be related to the binding mechanism: the peptides and the GYF domain first attract each other by the long-range electrostatic interactions between the charged residues, and then the peptides bind or leave the binding interface of the GYF domain by this "screw-like" motion along the interface. In addition, such screw-like motions may allow for a kinetically favorable binding process by "stripping off water molecules" upon binding and/or unbinding. Furthermore, these sites might act as delocalized anchors within protein associations that rely on fast structural rearrangements within the context of eukaryotic signal transduction.

Consistency between NMR Experiments and Theoretical Calculations. Binding analysis of the GYF domain in regard to the mutant and wild-type peptides and chemical-shift changes mapping (see Figure 4b) show the most significant difference between the wild-type complex and the G8W mutant to be the "backward" chemical-shift changes of the backbone HN of Trp8. The chemical shifts of the N−H group are mostly influenced by the local environment, e.g., alteration of hydrogen-bond strength, weaker effects of internal geometry, or by covalently linked aromatic groups. Therefore, the "backward" chemical-shift change indicates that the local environment of Trp8 in the mutant complex is closer to the free form of the GYF domain. Theoretical methods of predicting chemical shifts are still not applicable for systems as used in the present study: for *ab initio*

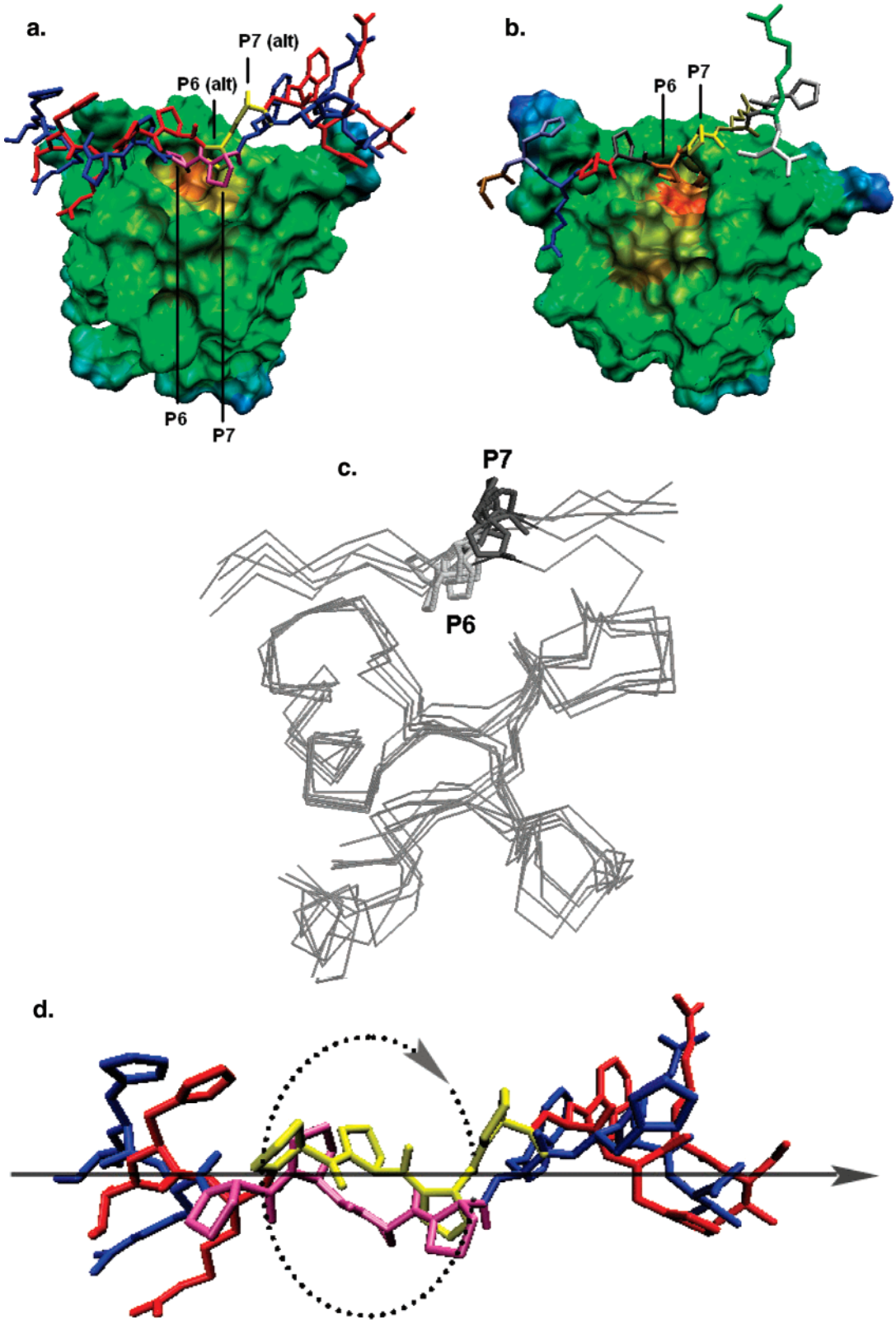

FIGURE 6: (a) Superposition of the two binding modes found in the simulation of the G8W mutant complex (starting from the docking results). The two conformations of the peptide are drawn as sticks (blue, mode 1; red, mode 2; pink, Pro6 and Pro7 in mode 1; yellow, Pro6 and Pro7 in mode 2). (b) Binding mode of the G8R mutant complex (representative conformation of the simulation). The peptide atoms are represented by sticks and colored according to their sequence number. In a and b, the GYF domain is represented by its molecular surface and colored by position (from orange to deep blue: completely buried to completely exposed) and Pro6 and Pro7 are labeled by their one-letter codes and sequence numbers. Mode 2 is labeled as "(alt)". (c) Superposition of the representative conformations of the five simulations of wild-type GYF complex starting from the alternative binding mode. Pro6 and Pro7 are represented by sticks and are labeled by their one-letter codes and sequence numbers. Pro6 is colored in light gray, and Pro7 is colored in dark gray. (d) Translation and rotation motions of the peptide between the two binding modes (blue, mode 1; red, mode 2; pink, Pro4 to Pro7 in mode 1; yellow, Pro4 to Pro7 in mode 2). For Pro4 to Pro7, a rotation is the principle component of motion, while for other residues in the peptide, a translation is the principle component of motion.

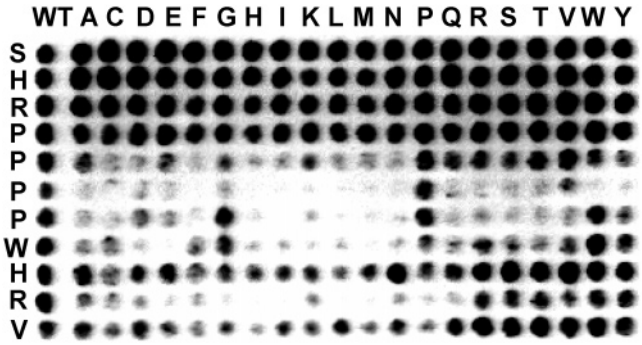

FIGURE 7: Substitution analysis of the SHRPPPPWHR peptide binding to the GYF domain. All single substitution analogues of the peptide were synthesized on a cellulose membrane. The single-letter code above each column marks the amino acid that replaces the corresponding wild-type residue, while the row defines the position of the substitution within the peptide. Spots in the most left column (WT) have identical sequences and represent the wild-type peptide. The membrane was incubated with a GST−GYF construct of CD2BP2. Bound protein was detected with an anti-GST primary antibody and a horseradish peroxidase coupled secondary antibody. The relative spot intensities correlate qualitatively with the binding affinities (*45*).

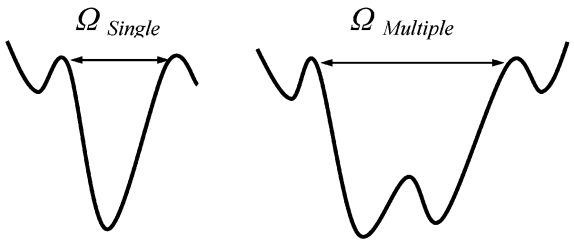

FIGURE 8: Funnel representation of the energy landscape for the binding of peptides to the GYF domain. On the left is the single-mode binding; on the right is multiple-mode binding. In the multiple-mode binding, the system can access significantly more states than in the single-mode binding and thus becomes entropically more favorable.

approaches, averaging of many conformations and including solvent effects for large systems is still too expensive, while for knowledge-based approaches, the required specificity may not be obtained (0.1 ppm of hydrogen) (*57*−*59*). Hence, direct comparison of the structure is more straightforward in this case. When looking at the structures of the free GYF domain (*10*), the wild-type complex (*14*), and the mutant complex (simulation), the backbone HN of Trp8 is exposed to the solvent (SASA > 0) in the free form of GYF domain while it is buried in the two complexes (wild-type and mutant). However, in the G8W mutant complex, an internal hydrogen bond is formed between the HN of Trp8 (domain) and the carbonyl oxygen of Pro6/Pro7 (peptide), with the distances between hydrogen and oxygen being 2.2 ± 0.3 Å. In the wild-type complex, no acceptor (oxygen atom) is found within 3.7 Å from the HN of Trp8 (domain). The newly formed hydrogen bond provides a similar local environment of the Trp8-HN of the GYF domain in the mutant complex as in the free form of the GYF domain. This is consistent with the "backward" chemical-shift change of the HN of Trp8 of the GYF domain.

The average intermolecular distances observed in the MD simulation of the wild-type complex started from the two different binding modes, and both are in agreement with the distance restraints derived from the NOE data that were used for the calculation of the experimental structure. The stability of both conformations in MD simulations suggests that these alternative binding modes are possible for the wild-type peptide. They may be hard to distinguish experimentally because the NMR distance restraints comply with both conformations.

CONCLUSIONS

Using molecular modeling and MD simulations, totaling 450 ns of simulation time, we studied the solvent conformation of the wild-type and mutant polyproline peptides that bind to the GYF domain. We found that the peptides formed PPII helix conformations even in absence of the GYF domain. These results agree well with recent experimental and theoretical studies on polypeptides with or without prolines and indicate that the formation of a PPII helix of the peptide is not induced by the binding processes alone.

On the basis of the simulations of the wild-type and mutated complexes and on our previous knowledge from NMR experimental studies of the GYF domain−ligand interaction, we modeled the general binding mode of polyproline peptides to the GYF domain. The hydrophobic interactions between the peptide residues Pro6 and Pro7 and binding pocket as well as the electrostatic attractions between the peptide residues Arg3 and Arg10 and the domain residues Glu31 and Glu9 play crucial roles in the binding.

Peptide docking and subsequent MD simulations of the G8X mutants identified an alternative binding mode, where a shift in register for the interacting prolines was observed. These results agree qualitatively well with NMR chemical-shift mapping experiments and indicate dynamic processes to be important for proline-rich sequence recognition. Possibly, such gliding motions along long proline-rich sequences decrease the entropic penalty of binding while still keeping a certain degree of specificity.

ACKNOWLEDGMENT

We thank Dr. Michael Hutter for critical comments on the manuscript, Angelika Ehrlich for membrane synthesis, and Michael Beyermann for the synthesis of peptides.

REFERENCES

1. Kay, B. K., Williamson, M. P., and Sudol, P. (2000) The importance of being proline: The interaction of proline-rich motifs in signaling proteins with their cognate domains, *FASEB J. 14*, 231−241.
2. Rubin, G. M., Yandell, M. D., Wortman, J. R., Miklos, G. L. G., Nelson, C. R., Hariharan, I. K., Fortini, M. E., Li, P. W., Apweiler, R., Fleischmann, W., Cherry, J. M., Henikoff, S., Skupski, M. P., Misra, S., Ashburner, M., Birney, E., Boguski, M. S., Brody, T., Brokstein, P., Celniker, S. E., Chervitz, S. A., Coates, D., Cravchik, A., Gabrielian, A., Galle, R. F., Gelbart, W. M., George, R. A., Goldstein, L. S. B., Gong, F. C., Guan, P., Harris, N. L., Hay, B. A., Hoskins, R. A., Li, J. Y., Li, Z. Y., Hynes, R. O., Jones, S. J. M., Kuehl, P. M., Lemaitre, B., Littleton, J. T., Morrison, D. K., Mungall, C., O'Farrell, P. H., Pickeral, O. K., Shue, C., Vosshall, L. B., Zhang, J., Zhao, Q., Zheng, X. Q. H., Zhong, F., Zhong, W. Y., Gibbs, R., Venter, J. C., Adams, M. D., and Lewis, S. (2000) Comparative genomics of the eukaryotes, *Science 287*, 2204−2215.
3. Zarrinpar, A., Bhattacharyya, R. P., and Lim, W. A. (2003) The structure and function of proline recognition domains, *Sci. STKE. RE8*.
4. Carlsson, L., Nystrom, L. E., Sundkvist, I., Markey, F., and Lindberg, U. (1977) Actin polymerizability is influenced by profilin, a low molecular weight protein in non-muscle cells, *J. Mol. Biol. 115*, 465−483.

5. Mayer, B. J., Hamaguchi, M., and Hanafusa, H. (1988) A novel viral oncogene with structural similarity to phospholipase C, *Nature 332*, 272−275.
6. Stahl, M. L., Ferenz, C. R., Kelleher, K. L., Kriz, R. W., and Knopf, J. L. (1988) Sequence similarity of phospholipase C with the non-catalytic region of src, *Nature 332*, 269−272.
7. Bork, P., and Sudol, M. (1994) The WW domain—A signaling site in dystrophin, *Trends Biochem. Sci. 19*, 531−533.
8. Niebuhr, K., Ebel, F., Frank, R., Reinhard, M., Domann, E., Carl, U. D., Walter, U., Gertler, F. B., Wehland, J., and Chakraborty, T. (1997) Novel proline-rich motif present in ActA of Listeria monocytogenes and cytoskeletal proteins is the ligand for the EVH1 domain, a protein module present in the Ena/VASP family, *EMBO J. 16*, 5433−5444.
9. Nishizawa, K., Freund, C., Li, J., Wagner, G., and Reinherz, E. L. (1998) Identification of a proline-binding motif regulating CD2-triggered T lymphocyte activation, *Proc. Natl. Acad. Sci. U.S.A. 95*, 14897−14902.
10. Freund, C., Dotsch, V., Nishizawa, K., Reinherz, E. L., and Wagner, G. (1999) The GYF domain is a novel structural fold that is involved in lymphoid signaling through proline-rich sequences, *Nat. Struct. Biol. 6*, 656−660.
11. Sancho, E., Vila, M. R., Sanchez-Pulido, L., Lozano, J. J., Paciucci, R., Nadal, M., Fox, M., Harvey, C., Bercovich, B., Loukili, N., Ciechanover, A., Lin, S. L., Sanz, F., Estivill, X., Valencia, A., and Thomson, T. M. (1998) Role of UEV-1, an inactive variant of the E2 ubiquitin-conjugating enzymes, in *in vitro* differentiation and cell cycle behavior of HT-29-M6 intestinal mucosecretory cells, *Mol. Cell. Biol. 18*, 576−589.
12. Pornillos, O., Alam, S. L., Davis, D. R., and Sundquist, W. I. (2002) Structure of the Tsg101 UEV domain in complex with the PTAP motif of the HIV-1 p6 protein, *Nat. Struct. Biol. 9*, 812−817.
13. Myllyharju, J., and Kivirikko, K. I. (1999) Identification of a novel proline-rich peptide-binding domain in prolyl 4-hydroxylase, *EMBO J. 18*, 306−312.
14. Freund, C., Kuhne, R., Yang, H. L., Park, S., Reinherz, E. L., and Wagner, G. (2002) Dynamic interaction of CD2 with the GYF and the SH3 domain of compartmentalized effector molecules, *EMBO J. 21*, 5985−5995.
15. Freund, C., Kuhne, R., Park, S., Thiemke, K., Reinherz, E. L., and Wagner, G. (2003) Structural investigations of a GYF domain covalently linked to a proline-rich peptide, *J. Biomol. NMR 27*, 143−149.
16. Wright, P. E., and Dyson, H. J. (1999) Intrinsically unstructured proteins: Re-assessing the protein structure−function paradigm, *J. Mol. Biol. 293*, 321−331.
17. Dunker, A. K., and Obradovic, Z. (2001) The protein trinity—Linking function and disorder, *Nat. Biotechnol. 19*, 805−806.
18. Dunker, A. K., Lawson, J. D., Brown, C. J., Williams, R. M., Romero, P., Oh, J. S., Oldfield, C. J., Campen, A. M., Ratliff, C. R., Hipps, K. W., Ausio, J., Nissen, M. S., Reeves, R., Kang, C. H., Kissinger, C. R., Bailey, R. W., Griswold, M. D., Chiu, M., Garner, E. C., and Obradovic, Z. (2001) Intrinsically disordered protein, *J. Mol. Graphics 19*, 26−59.
19. Verkhivker, G. M., Bouzida, D., Gehlhaar, D. K., Rejto, P. A., Freer, S. T., and Rose, P. W. (2003) Simulating disorder−order transitions in molecular recognition of unstructured proteins: Where folding meets binding, *Proc. Natl. Acad. Sci. U.S.A. 100*, 5148−5153.
20. Dyson, H. J., and Wright, P. E. (2002) Coupling of folding and binding for unstructured proteins, *Curr. Opin. Struct. Biol. 12*, 54−60.
21. Hamburger, J. B., Ferreon, J. C., Whitten, S. T., and Hilser, V. J. (2004) Thermodynamic mechanism and consequences of the polyproline II (P(II)) structural bias in the denatured states of proteins, *Biochemistry 43*, 9790−9799.
22. Blanco, F. J., Rivas, G., and Serrano, L. (1994) A short linear peptide that folds into a native stable β-hairpin in aqueous solution, *Nat. Struct. Biol. 1*, 584−590.
23. Vila, J. A., Baldoni, H. A., Ripoll, D. R., Ghosh, A., and Scheraga, H. A. (2004) Polyproline II helix conformation in a proline-rich environment: A theoretical study, *Biophys. J. 86*, 731−742.
24. Rucker, A. L., Pager, C. T., Campbell, M. N., Qualls, J. E., and Creamer, T. P. (2003) Host−guest scale of left-handed polyproline II helix formation, *Proteins 53*, 68−75.
25. Kelly, M. A., Chellgren, B. W., Rucker, A. L., Troutman, J. M., Fried, M. G., Miller, A. F., and Creamer, T. P. (2001) Host−guest study of left-handed polyproline II helix formation, *Biochemistry 40*, 14376−14383.
26. Williamson, M. P. (1994) The structure and function of proline-rich regions in proteins, *Biochem. J. 297*, 249−260.
27. Shi, Z. S., Olson, C. A., Rose, G. D., Baldwin, R. L., and Kallenbach, N. R. (2002) Polyproline II structure in a sequence of seven alanine residues, *Proc. Natl. Acad. Sci. U.S.A. 99*, 9190−9195.
28. Rucker, A. L., and Creamer, T. P. (2002) Polyproline II helical structure in protein unfolded states: Lysine peptides revisited, *Protein Sci. 11*, 980−985.
29. Woody, R. W. (1992) Circular dichroism and conformation of unordered polypeptides, *Adv. Biophys. Chem. 2*, 37−79.
30. Tiffany, M. L., and Krimm, S. (1972) Effect of temperature on the circular dichroism spectra of polypeptides in the extended state, *Biopolymers 11*, 2309−2316.
31. Tiffany, M. L., and Krimm, S. (1968) Circular dichroism of poly-L-proline in an unordered conformation, *Biopolymers 6*, 1767−1770.
32. Asher, S. A., Mikhonin, A. V., and Bykov, S. (2004) UV Raman demonstrates that α-helical polyalanine peptides melt to polyproline II conformations, *J. Am. Chem. Soc. 126*, 8433−8440.
33. Kentsis, A., Mezei, M., Gindin, T., and Osman, R. (2004) Unfolded state of polyalanine is a segmented polyproline II helix, *Proteins 55*, 493−501.
34. Mezei, M., Fleming, P. J., Srinivasan, R., and Rose, G. D. (2004) Polyproline II helix is the preferred conformation for unfolded polyalanine in water, *Proteins 55*, 502−507.
35. Chellgren, B. W., and Creamer, T. P. (2004) Short sequences of non-proline residues can adopt the polyproline II helical conformation, *Biochemistry 43*, 5864−5869.
36. Creamer, T. P. (1998) Left-handed polyproline II helix formation is (very) locally driven, *Proteins 33*, 218−226.
37. Sreerama, N., and Woody, R. W. (1999) Molecular dynamics simulations of polypeptide conformations in water: A comparison of α, β, and poly(Pro)II conformations, *Proteins 36*, 400−406.
38. Pappu, R. V., and Rose, G. D. (2002) A simple model for polyproline II structure in unfolded states of alanine-based peptides, *Protein Sci. 11*, 2437−2455.
39. Stapley, B. J., and Creamer, T. P. (1999) A survey of left-handed polyproline II helices, *Protein Sci. 8*, 587−595.
40. Kofler, M., Heuer, K., Zech, T., and Freund, C. (2004) Recognition sequences for the GYF domain reveal a possible spliceosomal function of CD2BP2, *J. Biol. Chem. 279*, 28292−28297.
41. Feng, S. B., Chen, J. K., Yu, H. T., Simon, J. A., and Schreiber, S. L. (1994) 2 binding orientations for peptides to the src SH3 domain—Development of a general model for SH3−ligand interactions, *Science 266*, 1241−1247.
42. Goddard, T. D., and Kneller, D. G. SPARKY 3, University of California, San Francisco, CA.
43. Frank, R. (1992) Spot-synthesis—An easy technique for the positionally addressable, parallel chemical synthesis on a membrane support, *Tetrahedron 48*, 9217−9232.
44. Kramer, A., and Schneider-Mergener J. (1998) Synthesis and screening of peptide libraries on continuous cellulose membrane supports, *Methods Mol. Biol. 87*, 25−39.
45. Kramer, A., Reineke, U., Dong, L., Hoffmann, B., Hoffmuller, U., Winkler, D., Volkmer-Engert, R., and Schneider-Mergener, J. (1999) Spot synthesis: Observations and optimizations, *J. Pept. Res. 54*, 319−327.
46. Heuer, K., Kofler, M. Langdon, M., Thiemke, K., and Freund, C. (2004) Structure of a helically extended SH3 domain of the T cell adapter protein ADAP. *Structure 12*, 603−610.
47. van der Spoel, D., van Drunen, R., and Berendsen, H. J. C. (1994) Groningen machine for chemical simulation, Department of Biophysical Chemistry, BIOSON Research Institute Nijenborgh 4 NL-9717 AG Groningen, The Netherlands.
48. Jorgensen, W. L., Maxwell, D. S., and TiradoRives, J. (1996) Development and testing of the OPLS all-atom force field on conformational energetics and properties of organic liquids, *J. Am. Chem. Soc. 118*, 11225−11236.
49. Ren, P. Y., and Ponder, J. W. (2003) Polarizable atomic multipole water model for molecular mechanics simulation, *J. Phys. Chem. B 107*, 5933−5947.
50. Jorgensen, W. L., Chandrasekhar, J., Madura, J. D., Impey, R. W., and Klein, M. L. (1983) Comparison of simple potential functions for simulating liquid water, *J. Chem. Phys. 79*, 926−935.

51. Hess, B., Bekker, H., Berendsen, H. J. C., and Fraaije, J. (1997) LINCS: A linear constraint solver for molecular simulations, *J. Comput. Chem. 18*, 1463−1472.
52. Essmann, U., Perera, L., Berkowitz, M. L., Darden, T., Lee, H., and Pedersen, L. G. (1995) A smooth particle mesh Ewald method, *J. Chem. Phys. 103*, 8577−8593.
53. Berendsen, H. J. C., Postma, J. P. M., van Gunsteren, W. F., DiNola, A., and Haak, J. R. (1984) Molecular dynamics with coupling to an external bath, *J. Chem. Phys. 81*, 684−3690.
54. Rarey, M., Kramer, B., Lengauer, T., and Klebe, G. (1996) A fast flexible docking method using an incremental construction algorithm, *J. Mol. Biol. 261*, 470−489.
55. Cowan, P. M., McGavin, S., and North, A. C. (1955) The polypeptide chain configuration of collagen, *Nature 176*, 1062−1064.
56. Parker, D., Rivera, M., Zor, T., Henrion-Caude, A., Radhakrishnan, I., Kumar, A., Shapiro, L. H., Wright, P. E., Montminy, M., and Brindle, P. K. (1999) Role of secondary structure in discrimination between constitutive and inducible activators, *Mol. Cell. Biol. 19*, 5601−5607.
57. Neal, S., Nip, A. M., Zhang, H. Y., and Wishart, D. S. (2003) Rapid and accurate calculation of protein H-1, C-13, and N-15 chemical shifts, *J. Biomol. NMR 26*, 215−240.
58. Meiler, J. (2003) PROSHIFT: Protein chemical shift prediction using artificial neural networks, *J. Biomol. NMR 26*, 25−37.
59. Gronwald, W., Boyko, R. F., Sonnichsen, F. D., Wishart, D. S., and Sykes, B. D. (1997) ORB, a homology-based program for the prediction of protein NMR chemical shifts, *J. Biomol. NMR 10*, 165−179.
60. Humphrey, W., Dalke, A., and Schulten, K. (1996) VMD: Visual molecular dynamics, *J. Mol. Graphics 14*, 33−38.

BI0479914